Chapter

In Silico Molecular Docking of Indonesian Medicinal Plants: *Garcinia mangostana, Eurycoma longifolia, Brucea javanica* and *Momordica charantia* as Neuraminidase Inhibitors Against H5N1

Ezekiel Hariara Gintar Sembiring Meliala, Eufrasia Cicero Siswan, Evelyn Catrina Sudianto, Frederick Jason, Gracella Fidelia, Finley Jakov Jap, Freya Medelline, Fachrul Hafiziva and Arli Aditya Parikesit

Abstract

Avian flu H5N1 remains an important world health concern due to its prevalence in poultry farming and mortality rate among humans. Its impact has been worsened by its resistance to inhibitors such as oseltamivir and peramivir. In this chapter, we explore the potential of natural compounds from Indonesian medicinal plants such as *Garcinia mangostana, Eurycoma longifolia, Brucea javanica,* and *Momordica charantia* as new neuraminidase inhibitors through molecular docking. Using the blind docking method on Galaxy, we determine the binding affinities of major phytoconstituents to H5N1 neuraminidase. The study found that gamma-mangostin from *G. mangostana* and Kuguacin J from *M. charantia* had greater predicted binding affinities compared to other reference compounds. Although the study is limited as it is done in silico, it has provided an understanding of the potential of natural compounds from Indonesian medicinal plants as an alternative to known antivirals.

Keywords: molecular docking, neuraminidase, H5N1, natural compounds, antiviral drug

1. Introduction

The H5N1 avian influenza virus, characterized by its high virulence, primarily infects birds and exhibits high contagiousness. This has resulted in significant outbreaks that have led to the culling of millions of poultry [1]. A systematic analysis of outbreaks spanning from 2010 to 2016 revealed H5N1 as the most prevalent subtype, predominantly affecting commercial poultry operations [2]. Since then, the virus has rapidly disseminated across Asia, Africa, Europe, and North America, causing widespread outbreaks and resulting in the demise of millions of birds [3]. In 2024, a novel H5N1 outbreak was reported in dairy cattle within the United States, necessitating heightened surveillance and biosecurity measures to mitigate the risk of human transmission [4]. The virus poses a grave pandemic threat, as it possesses the capability to infect humans and exhibits a mortality rate of approximately 60% among infected individuals. Although candidate vaccines have been developed, their widespread availability remains a challenge. Consequently, oseltamivir continues to be the preferred treatment for human cases [5].

Oseltamivir and zanamivir, neuraminidase inhibitors, are commonly used for influenza treatment and prevention. Both medications effectively alleviate symptoms, with preventive rates spanning from 60% to 90% [6]. Oseltamivir and zanamivir are effective against H5N1 influenza infections. While oseltamivir is widely employed, zanamivir exhibits promise due to its potency against H5N1 and its efficacy against oseltamivir-resistant strains [7]. However, zanamivir resistance can develop under specific conditions. In vitro studies indicate that mutations, such as at the Q136 residue of neuraminidase, can diminish the virus's sensitivity to zanamivir [8]. Although these mutations often arise in laboratory settings, prolonged antiviral use, particularly in immunocompromised patients, may also contribute to the development of resistant strains [9]. This evidence underscores the necessity for a novel neuraminidase inhibitor with enhanced potency against H5N1 outbreaks in humans. Molecular docking could be employed for screening potential neuraminidase inhibitors, as it offers enhanced reliability and efficiency in drug discovery [10]. Potential alternatives may be found in several indigenous plants in Indonesia, which demonstrate anti-neuraminidase activity. These include *G. mangostana, E. longifolia, B. javanica*, and *M. charantia* [11]. Thus, searching for alternative drugs from these plants may be a critical step in finding drugs to which the virus is not resistant.

This project focuses on identifying potential neuraminidase inhibitors from active compounds found in several selected plants commonly found in Indonesia. Molecular docking methods were employed to evaluate the binding affinity of active compounds, including *G. mangostana, E. longifolia, B. javanica*, and *M. charantia*, against the H5N1 neuraminidase enzyme. The primary objective of this study was to assess their potential as antiviral agents. The research aims to identify a potent neuraminidase inhibitor capable of treating influenza, particularly infections caused by H5N1, as a preventive measure against a potential pandemic, with molecular docking used to expedite drug discovery.

2. Methodology

2.1 Preparation of the ligands and receptors

The drugs oseltamivir and peramivir are known to effectively inhibit neuraminidase [12]. Through this activity, they can be used as H5N1 antivirals [7]. Thus, since the inhibition of H5N1 neuraminidase allows for the treatment of the infection, literature was reviewed to find compounds originating from Southeast Asian medicinal plants that are known to exhibit anti-neuraminidase activity. These candidates were sourced from *G. mangostana, E. longifolia, B. javanica*, and *M. charantia*, which are tropical plants commonly found in Southeast Asia and are known to exhibit moderate anti-H5N1 neuraminidase activity [11]. The ligands mentioned in the reviewed paper were obtained from PubChem and prepared for docking using Galaxy and the tools the platform provides [13, 14]. The selected ligands' structures can be seen in **Figure 1**.

Meanwhile, the H5N1 neuraminidase's structure was obtained from the Protein Data Bank (PDB). The potential receptor structures were screened to ensure they had sufficient resolution. This is because resolutions quantify the level of uncertainty associated with an atom; consequently, lower resolutions (in Å) signify more precise structures [15]. Following the search, the PDB entry "2HTY" was identified as meeting this criterion [16]. The receptor was then inspected using PyMol and prepared with the tools available within Galaxy [17–19].

2.2 Molecular docking

With the ligands and receptors prepared, molecular docking was conducted. The method employed was blind docking, which enables the entire surface of the receptor to be searched for binding sites, albeit with reduced accuracy compared to other methods [20]. Molecular docking was performed using the appropriate grid box in Galaxy [21, 22]. Other tools within the same platform were utilized to refine the results [23, 24]. With the docking results in an accessible format, the top three positions of each ligand with the highest binding affinities were selected for further analysis. They were compared to each other and the positive controls based on their binding affinities and their obtained RMSD values.

2.3 Post-docking validation

After docking, a protein-ligand complex's binding flexibility can be assessed using molecular dynamics (MD). In this study, the selected complexes were simulated through the use of CABS-Flex 3.0 [25]. The results of the simulation are root mean square fluctuations (RMSFs), which are used to quantify flexibility [26]. In addition to MD, the selected ligands must be validated by predicting whether their properties are conducive to their use as drugs. This study predicted the selected ligands' ADME-Tox properties using pkCSM [27].

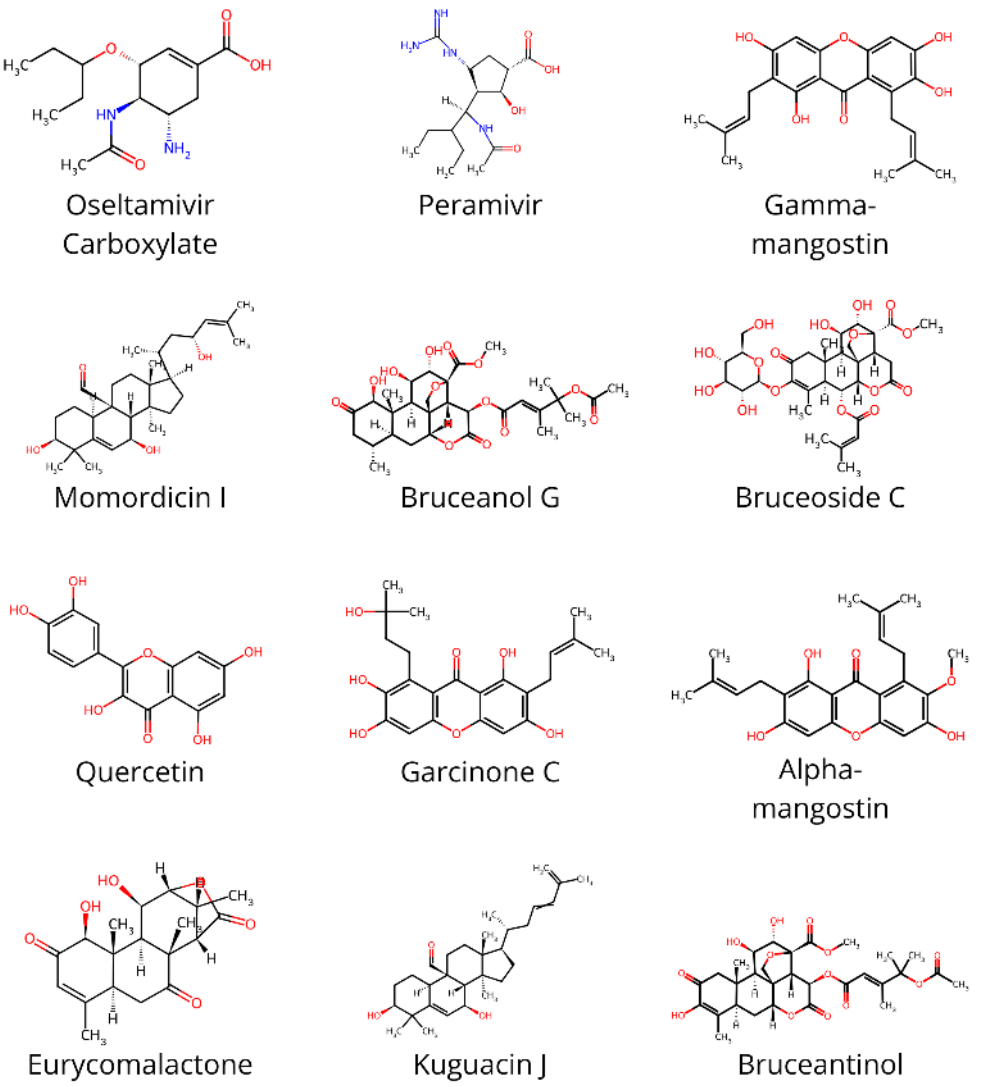


Figure 1.
Selected ligands.

3. Results and discussion

3.1 Results

PyMOL was used to inspect the protein and obtain its center. The center of the receptor, as seen through PyMOL, is shown in **Figure 2**.

A white-colored cross highlights the receptor's center. **Table 1** displays the obtained coordinates.

Once the receptor and ligands were prepared, docking was conducted in Galaxy. The positive controls were used to check the reliability of the docking simulation and

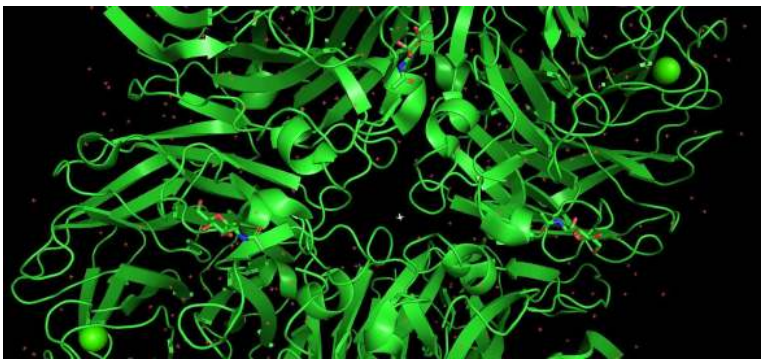


Figure 2.
Chosen center of the neuraminidase receptor in PyMOL.

X	Y	Z
3.605	47.024	103.945

Table 1.
Center coordinates.

to compare the binding affinities of antiviral candidates. The results of the positive controls' docking are shown in **Table 2**.

The candidate compounds were also simulated using molecular docking, and the results of the simulations are shown in **Table 3**.

After docking, the RMSF values of the ligand-protein complexes were obtained using CABS-Flex 3.0 to assess the stability of the complexes. A summary of the MD simulation results is presented in **Table 4**.

Table 4 shows the RMSF results of the H5N1 complexes to which the selected natural ligands were bound. The first column displays the ligand to which the complex is bound. The second column presents the average RMSF of the residues across all chains, while the third and fourth columns indicate the smallest and largest residue RMSF, respectively. In addition to assessing the binding stability using RMSF, the suitability of the ligands as drugs was evaluated by

Ligand	Model	Binding affinity (kcal/mol)	RMSD_LB	RMSD_UB
	1	−6.45	0	0
Oseltamivir Carboxylate	2	−6.28	1.932	4.011
	4	−5.953	17.266	19.892
	1	−6.093	0	0
Peramivir	2	−6.003	42.137	44.07
	3	−5.906	31.106	33.292

Table 2.
Positive control blind docking results.

Ligand	Plant origin	Model	Binding affinity (kcal/mol)	RMSD_LB	RMSD_UB
		1	−9.713	0	0
Gamma-mangostin	*G. mangostana*	2	−9.661	3.656	7.813
		3	−9.618	2.418	3.852
		1	−8.557	0	0
Quercetin	*B. javanica*	2	−8.555	26.258	28.748
		3	−8.509	28.771	31.274
		1	−8,039	0	0
Garcinone C	*G. mangostana*	2	−7,994	5,193	7,199
		4	−7,872	2,572	3,719
		1	−7.94	0	0
Alpha-mangostin	*G. mangostana*	2	−7.695	5.18	9.699
		6	−7.578	27.815	32.374
		1	−7.661	0	0
Momordicin I	*M. Charantia*	2	−7.592	4.538	7.345
		6	−6.957	21.135	23.894
		1	−7.401	0	0
Bruceanol G	*B. javanica*	2	−7.584	5.769	8.488
		7	−7.187	24.83	28.472
		1	−7.401	0	0
Bruceoside C	*B. javanica*	2	−7.327	1.857	3.508
		3	−7.298	22.309	25.548
		1	−7.088	0	0
Eurycomalactone	*E. longifolia*	2	−6.922	27.107	29.963
		3	−6.757	26.625	29.806
		1	−7.35	0	0
Kuguacin J	*M. Charantia*	2	−7.16	4.973	7.878
		3	−7.119	3.25	5.948
		1	−7.247	0	0
Bruceantinol	*B. javanica*	2	−7.201	3.233	9.852
		6	−6.878	6.185	9.177

Table 3.
Plant ligand blind docking results.

predicting their ADME-Tox properties. The absorption prediction results are shown in **Table 5**.

Table 5 presents the absorption prediction results for the 10 natural ligands in each row. The columns beside the "Ligand" column display the results for each absorption model. Notably, the P-glycoprotein substrate column indicates that all the selected ligands were P-glycoprotein substrates. Meanwhile, the distribution prediction results are presented in **Table 6**.

Bound ligand	Average RMSF (Å)	Minimum RMSF (Å)	Maximum RMSF (Å)
Gamma-mangostin	0.787	0.060	5.401
Quercetin	0.756	0.056	6.887
Garcinone C	0.830	0.060	6.339
Alpha-mangostin	0.810	0.058	7.282
Momordicin I	0.811	0.078	6.015
Bruceanol G	0.782	0.069	4.981
Bruceoside C	0.744	0.063	5.757
Eurycomalactone	0.805	0.054	7.067
Kuguacin J	0.762	0.061	5.113
Bruceantinol	0.713	0.049	5.595

Table 4.
Natural ligand-h5n1 RMSF summary.

Table 6 shows the distribution prediction for each ligand. As before, the ligands are presented by row, while the model results are presented by column. In addition to distribution, the metabolic properties of the ligands were predicted. The results are shown in **Table 7**.

Table 7 shows the metabolism prediction for each ligand. The ligands are presented by row, while the type of interaction each ligand has with an enzyme in the Cytochrome P450 family is shown in the columns. According to **Table 7**, there appears to be no type of enzyme interaction that all the ligands share. Following this, the excretion results were predicted, and the results are shown in **Table 8**.

Table 8 shows the excretion prediction for each ligand. The ligands are presented by row, while the results of the two excretion prediction models are presented in the columns. As shown in **Table 8**, all the ligands appear not to be renal OPCT12 substrates. The toxic properties of the ligands were predicted, as shown in **Table 9**.

Table 9 shows the toxicity prediction for each ligand. The ligands are presented by row, while the results of the toxicity prediction models are shown per column. As shown in **Table 9**, all ligands share the common property of not being hERG I inhibitors and not eliciting skin sensitization.

3.2 Discussion

3.2.1 Docking coordinates

The center coordinates for constructing docking box parameters were determined using PyMOL, an open-source software tool for visualizing macromolecules [28]. As indicated in **Table 1**, the center coordinates were 3.605, 47.024, and 103.945. Utilizing these coordinates as the center, a docking box suitable for blind docking can be designed by setting its dimensions to encompass the entire receptor [20].

Ligand	Water solubility (log mol/L)	$CaCo_2$ permeability (log Papp in 10-6 cm/s)	Intestinal absorption (human)(% Absorbed)	Skin permeability (log Kp)	P-glycoprotein substrate (Yes/No)	P-glycoprotein I inhibitor (Yes/No)	P-glycoprotein II inhibitor (Yes/No)
Gamma-mangostin	−4.567	0.762	89.268	−2.736	Yes	Yes	Yes
Quercetin	−3.275	0.076	73.104	−3.368	Yes	No	No
Garcinone C	−4.781	0.44	74.508	−3.197	Yes	Yes	Yes
Alpha-mangostin	−5.762	0.794	87.945	−3.23	Yes	Yes	Yes
Momordicin I	−5.987	1.174	91.498	−3.371	Yes	Yes	Yes
Bruceanol G	−4.219	−0.38	64.933	−2.815	Yes	Yes	No
Bruceoside C	−4.245	−0.375	64.797	−2.821	Yes	Yes	No
Eurycomalactone	−3.24	0.218	81.858	−4.139	Yes	No	No
Kuguacin J	−6.553	1.277	93.36	−3.28	Yes	Yes	Yes
Bruceantinol	−4.328	−0.431	68.796	−2.817	Yes	Yes	No

Table 5.
Absorption prediction result.

Ligand	VDss (human) (log L/kg)	Fraction unbound (human)(Fu)	BBB permeability (log BB)	CNS permeability (log PS)
Gamma-mangostin	−0.352	0.081	−0.967	−1.987
Quercetin	−1.133	0.275	−1.065	−3.071
Garcinone C	−0.744	0.106	−1.105	−2.9
Alpha-mangostin	−0.557	0	−0.969	−1.879
Momordicin I	0.588	0.021	−0.588	−1.964
Bruceanol G	−0.865	0.376	−1.882	−4.321
Bruceoside C	−0.874	0.373	−1.841	−4.284
Eurycomalactone	−0.057	0.42	−0.389	−3.307
Kuguacin J	0.782	0	0.144	−1.597
Bruceantinol	−0.849	0.355	−1.996	−4.215

Table 6.
Distribution prediction result.

Ligand	CYP2D6 substrate (Yes/No)	CYP3A4 substrate (Yes/No)	CYP1A2 inhibitor (Yes/No)	CYP2C19 inhibitor (Yes/No)	CYP2C9 inhibitor (Yes/No)	CYP2D6 inhibitor (Yes/No)	CYP3A4 inhibitor (Yes/No)
Gamma-mangostin	No	No	Yes	Yes	Yes	No	Yes
Quercetin	No	No	Yes	No	No	No	No
Garcinone C	No	Yes	No	No	No	No	No
Alpha-mangostin	No	Yes	No	Yes	Yes	No	Yes
Momordicin I	No	Yes	No	No	No	No	Yes
Bruceanol G	No	Yes	No	No	No	No	No
Bruceoside C	No	Yes	No	No	No	No	No
Eurycomalactone	No	Yes	No	No	No	No	No
Kuguacin J	No	Yes	No	No	No	No	No
Bruceantinol	No	Yes	No	No	No	No	No

Table 7.
Metabolism prediction result.

3.2.2 Positive control docking

To validate the docking setup and establish a benchmark for evaluating novel inhibitors, two clinically approved neuraminidase inhibitors, oseltamivir and peramivir, were selected as positive controls. These positive controls serve as a benchmark for evaluating the binding performance of the tested natural compound based on the predicted free binding energy [29].

The initial molecular docking experiment used oseltamivir carboxylate as a positive control. This is an active metabolite of oseltamivir, capable of binding and

Ligand	Total clearance (log mL/min/kg)	Renal OCT2 substrate (Yes/No)
Gamma-mangostin	0.559	No
Quercetin	0.488	No
Garcinone C	0.252	No
Alpha-mangostin	0.457	No
Momordicin I	0.396	No
Bruceanol G	0.3	No
Bruceoside C	0.323	No
Eurycomalactone	0.561	No
Kuguacin J	0.45	No
Bruceantinol	0.163	No

Table 8.
Excretion prediction result.

inhibiting influenza virus neuraminidases in vivo [30]. The results presented in **Table 2** demonstrate that oseltamivir carboxylate exhibits a superior binding affinity (−6.45 kcal/mol) compared to the second positive control model, peramivir, which possesses a binding affinity of −6.093 kcal/mol. This is because a lower free energy indicates a more stable binding complex between the ligand and neuraminidase [Kurczab, 2017]. Thus, these findings indicate that oseltamivir carboxylate facilitates a more stable binding toward H5N1 influenza neuraminidase and functions as a more effective neuraminidase inhibitor compared to peramivir. Notably, this result aligns with the findings of Liu et al. [31], which reported a comparable binding energy result of approximately −6.91 kcal/mol for avian influenza neuraminidase.

Furthermore, Tao et al. [32] reported that oseltamivir carboxylate establishes a direct hydrogen bond with the amino acid side chain R118 (Arg118). However, MD simulations indicate that under physiological conditions, protein structure undergoes alterations, potentially disrupting the direct hydrogen bond and replacing it with a weaker water-mediated hydrogen bond. This suggests that while oseltamivir carboxylate exhibits the highest binding affinity compared to peramivir as a positive control, its binding strength may be reduced under physiological conditions. Additionally, it is crucial to consider natural mutations in the H5N1 neuraminidase gene that can further impact binding compatibility with oseltamivir carboxylate. A study by Yadav et al. [33] identified the I117V mutation in the H5N1 neuraminidase gene. This was followed up by Mhlongo and Soliman [34], who revealed that the I117V mutant complex formed fewer hydrogen bonds and did not interact with the Glu37 residue, resulting in structural instability, distortion of oseltamivir, and a diminished binding affinity.

3.2.3 Natural ligand docking

The results for the potential neuraminidase inhibitor are presented in **Table 3**. Gamma-mangostin from *G. mangostana* emerges as the most promising

Ligand	AMES toxicity (Yes/No)	Max. tolerated dose (human) (log mg/kg/day)	hERG I inhibitor (Yes/No)	CYP2C19 inhibitor (Yes/No)	hERG II inhibitor (Yes/No)	Oral Rat Acute Toxicity (LD50) (mol/kg)	Oral Rat Chronic Toxicity (LOAEL) (log mg/kg_bw/day)	Hepatotoxicity (Yes/No)	Skin Sensitization (Yes/No)	*T. Pyriformis* toxicity (log ug/L)	Minnow toxicity (log mM)
Gamma-mangostin	No	0.414	No	Yes	Yes	1.701	1.82	No	No	0.308	−1.459
Quercetin	Yes	0.984	No	No	No	2.251	1.984	No	No	0.418	2.487
Garcinone C	No	0.717	No	No	Yes	2.415	2.282	No	No	0.443	0.711
Alpha-mangostin	No	0.833	No	Yes	No	2.452	2.146	No	No	0.746	−0.246
Momordicin I	No	−0.034	No	No	No	2.119	1.908	No	No	0.554	−1.575
Bruceanol G	No	−0.817	No	No	No	1.761	1.745	No	No	0.285	1.771
Bruceoside C	No	−0.841	No	No	No	1.786	1.765	No	No	0.285	1.862
Eurycomalactone	Yes	−0.185	No	No	Yes	1.975	1.653	No	No	0.448	1.776
Kuguacin J	No	0.072	No	No	No	2.138	1.966	Yes	No	0.729	−1.769
Bruceantinol	No	−0.873	No	No	No	1.865	1.666	No	No	0.285	1.585

Table 9.
Toxicity prediction result.

candidate due to its binding affinity of –9.713 kcal/mol, which is the lowest among all the results. However, the RMSD values of the two other selected models exceed 2 Å, indicating instability [35].

In comparison to the positive controls (oseltamivir and peramivir) presented in **Table 2**, Gamma-mangostin and Kuguacin J demonstrated greater predicted binding affinity and docking stability. These findings suggest that Kuguacin J and other plant-derived substances hold promise for further research and validation. Notably, the binding affinities of Kuguacin J surpass those of conventional antiviral controls such as oseltamivir and peramivir, which range from –5.953 to –6.45 kcal/mol. These results indicate that certain plant-derived substances may possess higher or equivalent inhibitory effects on neuraminidase compared to conventional medications.

In addition to Gamma-mangostin, several other compounds, as shown in **Table 3,** were identified as potential neuraminidase inhibitors. These include Alpha-mangostin and Garcinone C, both of which are xanthone derivatives found in the pericarp of G. mangostana. G. mangostana has been extensively studied for its pharmaceutical properties, including its antimicrobial activity [36].

The study found that Alpha-mangostin exhibited a binding affinity of –7.94 kcal/mol, suggesting a favorable interaction with the neuraminidase active site. However, its RMSD values exceeded 2 Å in models 2 and 3, indicating a lack of consistency in the predicted binding conformations. Garcinone C, on the other hand, demonstrated a slightly stronger binding affinity of –8.039 kcal/mol but exhibited less stable docking, as evidenced by the RMSD values of 3.711 Å for model 2 and 3.763 Å [35]. Thus, the presence of Alpha-mangostin, Garcinone C, and Gamma-mangostin within G. mangostana underscores its potential as a natural source of neuraminidase inhibitors.

Several other compounds sourced from *B. javanica*, as listed in **Table 3**, demonstrated binding compatibility with neuraminidase, including Bruceanol G, Bruceoside C, and Bruceantinol. These quassinoids are well-known constituents of *B. javanica*, a medicinal plant traditionally utilized in Southeast Asian herbal medicine. It is recognized for its pharmacological properties, particularly its anticancer, antimalarial, and anti-inflammatory effects [37–39]. The molecular docking analysis conducted in this study showed the highest binding affinities, ranging from –7.247 to –7.401 kcal/mol, indicating a favorable interaction with the neuraminidase active site. However, the RMSD values of all compounds originating from this plant, excluding model 2 of Bruceoside C, exceeded 2 Å, suggesting a lower consistency in the predicted binding conformations across docking models [35]. Bruceoside C in model 2 exhibited an RMSD value of 1.972 Å, indicating a more stable pose in that docking instance. Nevertheless, the overall docking behavior of Bruceanol G, Bruceoside C, and Bruceantinol underscores their potential as neuraminidase inhibitors.

Furthermore, Quercetin, a flavonoid also identified in B. javanica, exhibited a remarkable binding affinity of –8.557 kcal/mol, ranking among the more effective compounds in this study. In contrast to quassinoids, Quercetin is a flavonoid belonging to a class of polyphenolic compounds known for their antioxidant, anti-inflammatory, and antiviral properties, particularly against influenza viruses, as shown in numerous studies [40–42]. For instance, Mehrbod et al. [43] and Wu et al. [44] reported that Quercetin and its derivatives, such as isoQuercetin, inhibit influenza A virus replication by modulating viral entry

and suppressing neuraminidase activity. This aligns with the docking results of the present study, wherein Quercetin exhibited a strong predicted interaction with the neuraminidase active site. However, its RMSD values across binding modes were significantly above 2 Å, indicating substantial variability in pose stability. Nevertheless, the docking findings, in conjunction with existing literature, support the therapeutic potential of Quercetin as a neuraminidase inhibitor. Kuguacin J and Momordicin I, both derived from *M. charantia*, also demonstrate notable binding affinity toward neuraminidase, with values of −7.35 kcal/mol and −7.661 kcal/mol, respectively.

M. charantia, commonly known as bitter melon, is a widely utilized medicinal plant in Asia for its antidiabetic, antiviral, and anti-inflammatory properties [45]. While both compounds exhibited relatively strong binding potential, their docking results indicated RMSD values exceeding 2 Å, suggesting variability and diminished stability in their predicted binding conformations. The compound from *M. charantia*, Momordicin I, showed RMSD values of 4.538 Å in model 2 and 21.135 Å in model 6, respectively, indicating a significant deviation from the reference pose. These findings indicate that while the compounds may possess affinity toward the target, the absence of binding mode consistency limits their reliability without modifications.

Eurycomalactone, a quassinoid compound isolated from *E. longifolia*, demonstrated a binding affinity of −7.088 kcal/mol in the current molecular docking analysis, suggesting a potentially favorable interaction with the neuraminidase active site. Eurycomalactone is widely recognized for its diverse pharmacological activities, including anti-inflammatory and anticancer effects [46, 47]. Although its direct antiviral action has received less extensive research, the findings indicate that eurycomalactone may possess neuraminidase-inhibitory potential. However, all RMSD values recorded for its docking models were above 2 Å, indicating reduced conformational stability in this study. These findings suggest that further testing is necessary to ascertain its efficacy against the influenza virus.

The in silico molecular docking approach is widely recognized for its efficiency in conducting preliminary screening of binding affinity and pose stability of natural ligands against the neuraminidase active site [48]. These findings hold biological significance, as neuraminidase is a pivotal enzyme in the influenza virus life cycle [49]. By inhibiting this enzyme, viral release and transmission can be stopped. Furthermore, natural ligands derived from plants exhibiting high binding affinities and docking patterns demonstrate greater efficacy as antiviral agents against H5N1. Therefore, a collaboration between natural product research and computer sciences will help identify more treatment options that are effective and sustainable.

3.2.4 RMSF results

RMSF measures the movement of a single amino acid during a MD simulation, thus quantifying flexibility at the residue level [50]. In order to be considered stable, ligand-protein complexes must have protein backbone RMSF values below 2.5 Å. According to this metric, the average RMSF values of all H5N1-ligand complexes shown in **Table 4** (ranging from 0.713 to 0.830 Å) indicate that protein structures remained stable upon binding with selected natural ligands. Among these, the

Bruceantinol-bound complex exhibited the lowest mean RMSF, suggesting relatively reduced overall flexibility. Meanwhile, Garconone C showed the highest mean RMSF, though still well within the acceptable stability threshold.

Despite the overall stability indicated by the average RMSF values, the maximum RMSF values for several complexes exceeded 5 Å, with the Alpha-mangostin – and Eurycomalactone-bound complexes displaying the highest peak fluctuations. These elevated maximum RMSF values suggest that certain regions within the protein undergo localized instability. However, such high RMSF values are more commonly associated with solvent-exposed loop regions and terminal residues that are more flexible. This behavior has been observed in multiple MD studies, where fluctuating loop regions correspond to higher RMSF peaks [51]. Therefore, the presence of higher-than-acceptable maximum RMSF values does not necessarily reflect the instability of the ligand-binding cores, but rather normal dynamic behavior of flexible protein regions during the simulation.

3.2.5 Adme-tox results

Water solubility is an important property for drugs because it allows them to spread evenly in the body and work effectively. It is especially critical for effective oral delivery. Good water solubility also provides drugs with higher bioavailability and better chemical stability [52]. Compounds with solubility values ≥0 are classified as highly soluble; those with values between 0 and –2 are considered soluble; values ranging from –2 to –4 indicate slight solubility; and compounds with solubility values below –4 are regarded as insoluble [53]. Therefore, according to the defined standard, most of the compounds are not soluble, as most of their values were below –4. Caco-2 permeability is commonly regarded as the "gold standard" in vitro test for determining how much of a medicine would actually enter the human body after swallowing [54]. High-permeability drugs have Papp values between 13 and 76.7 × 10^{-6} cm/s, low-permeability drugs have Papp values below 0.74 × 10^{-6} cm/s, and moderate-permeability drugs fall between 1.29 and 16.0 × 10^{-6} cm/s. Based on **Table 5**, all ligands had low permeability values, as all the values stood below 1.29. Ligands with low Caco2 permeability (log Papp in 10^{-6} cm/s) may suggest poor absorption in the gastrointestinal system, which is potentially caused by restricted passive diffusion or other absorption processes [55]. Even so, low Caco-2 permeability might also imply a paracellular diffusion mechanism rather than transcellular diffusion or carrier-mediated transport [56]. As transdermal drug delivery systems rely on a medication's capacity to cross the skin barrier, the low values contraindicate the use of these compounds as skin-applied products. Compounds having a LogKp value greater than –2.5 cm/h have limited skin permeability [57]. Therefore, according to **Table 5**, all compounds had low skin permeability, as the values stood above the threshold. This suggests that the compounds had limited transdermal applications. As for the P-glycoprotein substrate, P-glycoprotein I inhibitor, and P-glycoprotein II inhibitor values, all ligands can be actively transported out of cells by P-gp. Meanwhile, most of the ligands can inhibit P-glycoprotein I, except for Quercetin and Eurycomalactone. On the other hand, half of the ligands, which include Gamma-mangostin, Garcinone C, Alpha-mangostin, Momordicin I, and Kuguacin J, can also inhibit P-glycoprotein II. As for HIA, it is a crucial

pharmacokinetic mechanism that determines the bioavailability of a medication or molecule after absorption in the small intestine [58]. A high value of HIA, HIA ≥30%, is considered to be well absorbed in the human intestine [59]. Therefore, it can be concluded that all of the proposed ligands are highly absorbable by the human intestine, as all the HIA values were above 60%, with the majority of them having HIA values above 70%, while the highest HIA percentage was achieved by Momordicin I.

VDss (human) refers to the human steady-state volume of distribution, where low VDss implies that the medicine spends the majority of its time in the bloodstream, which is important for treatments that target blood vessels, and high VDss suggests extensive tissue binding/partitioning is frequently observed with lipophilic substances or medicines that bind to intracellular proteins or fat. Generally, various thresholds are used to characterize distribution quantities as low, moderate, or large. Values can range from 0.04 L/kg (all compounds in plasma) to hundreds of L/kg (most compounds in tissue). Thresholds for designating compounds as "moderate" or "high" volume vary in the literature [60]. Based on **Table 6**, all values of VDss were below 1, and most were below 0. The ligand with the highest VDss value was Kuguacin J (0.782). A Fu value below 0.05 was considered low, while a value above 0.2 was considered high [61]. Therefore, it can be concluded that the majority of the ligands had moderate to high Fu levels, while two ligands, Alpha-mangostin and Kuguacin J, had a value of 0. According to previous findings, compounds with blood–brain barrier permeability (BBB +) generally have log BB values exceeding 0, whereas BBB-impermeable compounds display log BB values less than −0.3 [62]. Therefore, according to **Table 6**, all ligands except Kuguacin J are not able to pass the BBB (blood-brain barrier). For CNS permeability, compounds with log PS values greater than −2 are generally considered capable of penetrating the central nervous system, indicating higher blood–brain barrier permeability, whereas compounds with log PS values below −3 show poor CNS penetration and low BBB permeability [63]. Some of the ligands (e.g., Gamma-mangostin, Alpha-mangostin, Momordicin I, and Kuguacin J) have log PS values over −2, suggesting greater potential for central nervous system penetration. Several substances have log PS values below −3 (e.g., Quercetin, Bruceanol G, Bruceoside C, Eurycomalactone, and Bruceantinol), indicating minimal CNS permeability and blood-brain barrier penetration. The log BB measures the brain vs. blood concentrations at equilibrium, mixing the effects of distribution and binding, while log PS reflects the intrinsic permeability rate across the BBB before equilibrium [64]. For the metabolism precision result (refer to **Table 6**), none of the ligands are substrates of CYP2D6; most of them are substrates of CYP3A4, except for Gamma-mangostin and Quercetin; and the majority of them are inhibitors of CYP1A2, except for Gamma-mangostin and Quercetin. Additionally, most of them are not inhibitors of CYP2C19 and CYP2C9 except for Gamma-mangostin and Alpha-mangostin. All the ligands are inhibitors of CYP2D6, and only some of them (Gamma-mangostin, Alpha-mangostin, and Momordicin I) are inhibitors of CYP3A4.

As for the excretion prediction results, **Table 8** shows that none of the ligands acted as substrates to the renal OCT2. OCT2, or organic cation transporter 2, is an enzyme that functions in the initial step of cationic drug excretion [65]. Thus, drugs that are substrates to this enzyme are likely to be excreted through this process. Since none of the drugs act as an OCT2 substrate,

they are not likely to be excreted through this process. As for how well the drugs will be cleared from the body, this property can be quantified with total clearance. Drugs with a total clearance over 5 mL/min/kg, or around 0.699 log mL/min/kg, are considered to have a high clearance [66]. **Table 8** shows that none of the ligands reach this threshold, so they do not have high clearance. Additionally, drugs that do not act as OCT2 substrates but have high clearance are considered to have good bioavailability due to efficient metabolism and absorption [67]. All of the drugs pass the first property needed to be considered as having potentially good bioavailability, but none of them have what is considered high clearance.

Based on the data in **Table 9**, Quercetin and Eurycomalactone were found to exhibit AMES toxicity. Regarding organ safety, most compounds were predicted to be safe for the liver; however, Kuguacin J was identified as a potential hepatotoxin. Furthermore, none of the evaluated ligands or compounds were found to cause skin sensitization. The hERG gene encodes a potassium channel in the heart that regulates the heartbeat. Inhibition of these channels can cause long QT syndrome and potentially deadly cardiac arrhythmias [68]. From the results, almost all compounds were safe for the heart, as they did not inhibit both hERG I and hERG II, except for Gamma-mangostin, Garcinone C, and Eurycomalactone. CYP2C19 is a key enzyme in the liver that breaks down medicines. Blocking CYP2C19 inhibits the metabolism of other pharmaceuticals, which can lead to hazardous drug-drug interactions [69]. According to the results, only Gamma-mangostin and Garcinone C were known to inhibit CYP2C19.

3.2.6 Strengths and limitations of the study

The experimental findings demonstrated promising results in identifying ligands derived from indigenous plants in Indonesia as potent neuraminidase inhibitors. All proposed ligands exhibited greater binding affinity compared to positive controls, suggesting enhanced inhibition of H5N1 neuraminidase. These discoveries may advance the development of treatments for H5N1 infection, should it emerge as a global concern or pandemic in the future. The availability of suitable ligands sourced from locally occurring plants in Indonesia facilitates their extraction and manufacturing as drugs without concerns regarding resource scarcity.

The utilization of plants as drugs presents a renewable source of medicine with diverse therapeutic activities and structural characteristics. Furthermore, plant-derived compounds often exhibit enhanced stability, reduced side effects, and pleiotropic druggability compared to synthetic drugs [70].

Despite the high binding affinity of the ligands, several limitations arise from the application of blind docking. Blind docking encounters challenges in accuracy and efficiency due to the extensive search space involved. It may be less precise than targeted docking if the active site is well-defined and specific interactions are desired [38]. Furthermore, critical aspects affecting binding affinity predictions, including solvent effects and hydrogen bonding descriptions, were not incorporated in the experiment [48]. Lastly, the provided binding affinity and RMSD did not elucidate which molecules interacted with the receptor, and there is little knowledge regarding the precise molecular interactions between ligands and receptors.

3.2.7 Future suggestions

Given that all the ligands have been confirmed to bind with the protein through molecular docking and dynamics, density functional theory analyses can be conducted for a more precise prediction of their binding affinities. Density functional theory employs quantum mechanical calculations to model the electronic structures of compounds and provide realistic interactions between them [71]. However, in-silico methods solely provide predictions and, consequently, must undergo in vitro validation [29]. Therefore, with the knowledge that all of the tested natural compounds possess the capability of binding with H5N1 based on their binding affinities, future studies should validate these findings by analyzing their interactions with in vitro methods through the utilization of techniques such as isothermal titration calorimetry (ITC), high-throughput stability, mobility, or spectroscopic shift assays [17]. Conversely, the interaction of ligands with proteins can be experimentally determined by visualizing the structures of the components at an atomic level using methods like X-ray crystallography, nuclear magnetic resonance (NMR), Laue X-ray diffraction, small-angle X-ray scattering, and cryo-electron microscopy [28].

3.2.8 Future applications

The study revealed that herbal medicines, such as Gamma-mangostin and Kuguacin J, exhibit greater binding affinities and more stable docking postures compared to conventional antivirals like oseltamivir and peramivir. These molecules present novel avenues for drug development and discovery, with the potential for further validation through in vitro and in vivo research. Should these molecules prove effective, structural modifications can be undertaken to enhance their pharmacokinetic properties while mitigating potential toxicity. Furthermore, these compounds may be formulated into nasal sprays or inhalable devices for early-stage influenza intervention. As these compounds are derived from easily-accessible medicinal plants in Indonesia, they hold the potential to foster locally generated, cost-effective antiviral therapies, thereby improving medication accessibility in Indonesia. The integration of computational drug development with traditional ethnobotanical knowledge may lead to the identification of multi-target antiviral medications capable of effectively combating emerging influenza strains and bolstering global pandemic preparedness.

4. Conclusion and recommendations

This study sought to identify novel ligands as neuraminidase inhibitors for H5N1 avian influenza through molecular docking. Gamma-mangostin and Kuguacin J exhibited superior binding affinities compared to positive controls. Furthermore, the overall plant ligands demonstrated potential as neuraminidase inhibitors due to their docking results and binding stability. In addition, as the compounds used are derived from local flora, they will have greater overall relevance in Indonesia. Still, due to the in-silico nature of the study, these results require more rigorous validation. Future studies should include in vitro methods to validate the in silico data, such as isothermal titration calorimetry, high-throughput stability, mobility, and spectroscopic shift assays.

Acknowledgments

The authors extend their sincere gratitude to the Research and Community Service Department (LPPM) of i3L University for their invaluable support. Apple Intelligence was used to detect and revise any typographical errors or grammatical mistakes found in the initial draft of the manuscript.

Author details

Ezekiel Hariara Gintar Sembiring Meliala[1], Eufrasia Cicero Siswan[1], Evelyn Catrina Sudianto[1], Frederick Jason[1], Gracella Fidelia[1], Finley Jakov Jap[1], Freya Medelline[1], Fachrul Hafiziva[1] and Arli Aditya Parikesit[2*]

1 Department of Biomedicine, School of Health and Life Sciences, i3L University, Jakarta, Indonesia

2 Department of Biotechnology, School of Health and Life Sciences, i3L University, Jakarta, Indonesia

*Address all correspondence to: arli.parikesit@I3l.ac.id

IntechOpen

© 2026 The Author(s). Licensee IntechOpen. This chapter is distributed under the terms of the Creative Commons Attribution License (http://creativecommons.org/licenses/by/4.0/), which permits unrestricted use, distribution, and reproduction in any medium, provided the original work is properly cited. CC BY

References

[1] Graziosi G, Lupini C, Catelli E, Carnaccini S. Highly Pathogenic Avian Influenza (HPAI) H5 Clade 2.3.4.4b Virus Infection in Birds and Mammals. Animals. 2024;**14**(9):1372. https://www.mdpi.com/2076-2615/14/9/1372

[2] Chatziprodromidou IP, Arvanitidou M, Guitian J, Apostolou T, Vantarakis G, Vantarakis A. Global avian influenza outbreaks 2010–2016: A systematic review of their distribution, avian species and virus subtype. Systematic Reviews. 2018;**7**(1):17. DOI: 10.1186/s13643-018-0691-z

[3] Wille M, Barr IG. Resurgence of avian influenza virus. Science. 2022;**376**(6592):459–460

[4] Sah R, Srivastava S, Kumar S, Mehta R, Donovan S, Sierra-Carrero L, et al. Concerns on H5N1 avian influenza given the outbreak in U.S. dairy cattle. The Lancet Regional Health - Americas. 2024;**35**:100785–5

[5] Shrestha D, Bhattachan B, Parajuli H, Shrestha S. Avian/Bird flu: A review: H5N1 outbreaks in Nepal. Nepal Journal of Biotechnology. 2021;**9**(1):24–41

[6] Lehnert R, Pletz M, Reuss A, Schaberg T. Antiviral medications in seasonal and pandemic influenza. Deutsches Aerzteblatt Online. 2016;**113**(47). https://www.ncbi.nlm.nih.gov/pmc/articles/PMC5240024/

[7] Kawai N. How to use anti-influenza drugs: Zanamivir and Oseltamivir. In: Fujita J, editor. Influenza: Advances in Diagnosis and Management. Singapore: Springer Singapore; 2020;149–159

[8] Little K, Leang SK, Butler J, Baas C, Harrower B, Mosse JA, et al. Zanamivir-resistant influenza viruses with Q136K or Q136R neuraminidase residue mutat ions can arise during MDCK cell culture creating challenges for antiviral suscep tibility monitoring. Eurosurveillance. 2015;**20**(45):30060. DOI: 10.2807/1560-7917.ES.2015.20.45.30060

[9] Trebbien R, Pedersen SS, Vorborg K, Franck KT, Fischer TK. Development of oseltamivir and zanamivir resistance in influenza A (H1N1)pdm09 virus, Denmark, 2014. Eurosurveillance. 2017;**22**(3):30445. DOI: 10.2807/1560-7917.es.2017.22.3.30445

[10] Aguiar C, Camps I. Molecular docking in drug discovery: Techniques, applications, and advancements. Current Medicinal Chemistry. 2024;**32**(28):5924–5938. DOI: 10.2174/0109298673325827240926081845

[11] Ikram NKK, Durrant JD, Muchtaridi M, Zalaludin AS, Purwitasari N, Mohamed N, et al. A virtual screening approach for identifying plants with Anti H5N1 neuraminidase activity. Journal of Chemical Information and Modeling 2015;**55**:308–316

[12] Pascua PNQ, Chesnokov A, Nguyen HT, Di H, La Cruz JD, Jang Y, et al. Antiviral Susceptibility of Influenza A(H5N1) Clade 2.3.2.1c and 2.3.4.4b Viruses from Humans, 2023–2024. Emerging Infectious Diseases. 2025;**31**(4):751–760. DOI: 10.3201/eid3104.241820

[13] Afgan E, Nekrutenko A, Grüning BA, Blankenberg D, Goecks J, Schatz MC,

et al. The Galaxy platform for accessible, reproducible and collaborative biomedical analyses: 2022 update. Nucleic Acids Research. 2022;**50**(W1): W345–W351. DOI: 10.1093/nar/gkac247

[14] O'Boyle NM, Banck M, James CA, Morley C, Vandermeersch T, Hutchison GR. Open Babel: An open chemical toolbox. Journal of Cheminformatics. Internet. 2011;**3**(1). DOI: 10.1186/1758-2946-3-33

[15] Lohning AE, Levonis SM, Williams-Noonan B, Schweiker SS. A practical guide to molecular docking and homology modelling for medicinal chemists. Current Topics in Medicinal Chemistry. 2017;**17**(18):2023–2040. DOI: 10.2174/1568026617666170130110827

[16] Mitrasinovic PM. On the structure-based design of novel inhibitors of H5N1 influenza A virus neuraminidase (NA). Biophysical Chemistry. 2009;**140**(1-3):35–38

[17] Delano W. PyMOL: An open-source Molecular Graphics Tool. CCP4 Newsletter on Protein Crystallography. 2002;**40**(1):82–92

[18] Niksic H. GNU Wget 1.25.0. Boston: Free Software Foundation; 2024

[19] Dallakyan S. MGLTools [Internet]. MGLTools. 2021. Available from: https://ccsb.scripps.edu/mgltools/ [Accessed: 2025-June-20]

[20] Jofily P, Pascutti PG, Torres PHM. Improving blind docking in DOCK6 through an automated preliminary fragment probing strategy. Molecules. 2021;**26**(5):1224

[21] Narkhede RR, Cheke RS, Ambhore JP, Shinde SD. The molecular docking study of potential drug candidates showing anti-COVID-19 activity by exploring of therapeutic targets of SARS-CoV-2. Eurasian Journal of Medicine and Oncology. 2020;**4**(3):185–195

[22] Eberhardt J, Santos-Martins D, Tillack AF, Forli S. AutoDock Vina 1.2.0: New docking methods, expanded force field, and python bindings. Journal of Chemical Information and Modeling. 2021;**61**(8):3891–3898

[23] RDKit. The RDKit 2025.03.1 documentation [Internet]. Rdkit.org. 2025. Available from: https://rdkit.org/docs/ [Accessed: 2025-May-11]

[24] Free Software Foundation. Gawk-GNU Project-Free Software Foundation (FSF) [Internet]. Gnu.org. 2008. Available from: https://www.gnu.org/software/gawk/ [Accessed: 2025-May-11]

[25] Wróblewski K, Zalewski M, Kuriata A, Kmiecik S. CABS-flex 3.0: An online tool for simulating protein structural flexibility and peptide modeling. Nucleic Acids Research. 2025;**53**(W1):W95–W101. DOI: 10.1093/nar/gkaf412

[26] Song X, Bao L, Feng C, Huang Q, Zhang F, Gao X, et al. Accurate prediction of protein structural flexibility by deep learning integrating intricate atomic structures and cryo-EM density information. Nature Communications. 2024;**15**(1). https://pubmed.ncbi.nlm.nih.gov/38956032/

[27] Pires DEV, Blundell TL, Ascher DB. pkCSM: Predicting small-molecule pharmacokinetic and toxicity properties using graph-based signatures. Journal of Medicinal Chemistry. 2015;**58**(9):4066–4072. https://www.ncbi.nlm.nih.gov/pmc/articles/PMC4434528/#ref1

[28] DeLano WL, Bromberg S. PyMOL User's Guide. San Francisco: DeLano Scientific LLC; 2004

[29] Zothantluanga JH, Chetia D. A beginner's guide to molecular docking. Sciences of Phytochemistry. 2022;**1**(2):37–40

[30] Wade KC. Antiviral Dosing Considerations for Term and Preterm Infants. In: Benitz WE, Smith PB, editors. Infectious Disease and Pharmacology: Neonatology Questions and Controversies. Amsterdam: Elsevier; 2019. p. 193–205

[31] Liu Z, Zhao J, Li W, Wang X, Xu J, Xie J, et al. Molecular Docking of Potential Inhibitors for Influenza H7N9. Computational and Mathematical Methods in Medicine. 2015;**2015**:1–8

[32] Tao J, Wang H, Wang W, Mi N, Zhang W, Wen Q, et al. Binding mechanism of oseltamivir and influenza neuraminidase suggests perspectives for the design of new anti-influenza drugs. PLOS Computational Biology. 2022;**18**: e1010343

[33] Yadav M, Igarashi M, Yamamoto N. Theoretical insights into the molecular mechanism of I117V mutation in neuraminidase mediated reduction of oseltamivir drug susceptibility in A/H5N1 influenza virus. PeerJ Physical Chemistry. 2021;**3**:e19

[34] Mhlongo NN, Soliman MES. Single H5N1 influenza A neuraminidase mutation develops resistance to oseltamivir due to distorted conformational and drug binding landscape: Multiple molecular dynamics analyses. RSC Advances. 2015;**5**(14):10849–10861

[35] Guterres H, Im W. CHARMM-GUI -Based induced fit docking workflow to generate Reliable protein–ligand binding modes. Journal of Chemical Information and Modeling. 2023;**63** (15):4772–4779

[36] Rizaldy D, Hartati R, Nadhifa T, Fidrianny I. Chemical compounds and pharmacological activities of mangosteen *(Garcinia mangostana L.)* – Updated review. Biointerface Research in Applied Chemistry. 2021;**12**(2):2503–2516

[37] Chen J, Yu D, Li X, Deng Q, Yang H, Chen L, et al. A review of *Brucea javanica:* Metabolites, pharmacology and clinical application. Frontiers in Pharmacology. 2024;**14**:1317620. https://www.ncbi.nlm.nih.gov/pmc/articles/PMC10871038/

[38] Yoon BK, Lim ZY, Jeon WY, Cho NJ, Kim JH, Jackman JA. Medicinal activities and nanomedicine delivery strategies for *Brucea javanica* oil and its molecular components. Molecules. 2020;**25**(22):5414–4

[39] Zhang J, Xu HX, Dou YX, Huang QH, Xian YF, Lin ZX. Major Constituents From *Brucea javanica* and their pharmacological actions. Frontiers in Pharmacology. 2022;13. DOI: 10.3389/fphar.2022.853119

[40] Carrillo-Martinez EJ, Flores-Hernández FY, Salazar-Montes AM, Nario-Chaidez HF, Hernández-Ortega LD. Quercetin, a flavonoid with great pharmacological capacity. Molecules. 2024;**29**(5):1000. https://www.mdpi.com/1420-3049/29/5/1000

[41] Choubey SS, Gautam AS, Vaibhav L, Asthana S, Nanda A, Dey M, et al. Comparative in silico, in vitro and ex vivo anti-inflammatory activity of

Quercetin. MedComm – Future Medicine. 2023;**2**(3):e57. DOI: 10.1002/mef2.57

[42] Di Petrillo A, Orrù G, Fais A, Fantini MC. Quercetin and its derivates as antiviral potentials: A comprehensive review. Phytotherapy Research. 2021;**36**(1):266–278

[43] Mehrbod P, Hudy D, Shyntum D, Markowski J, Łos MJ, Ghavami S. Quercetin as a Natural therapeutic candidate for the treatment of influenza virus. Biomolecules. 2020;**11**(1):10

[44] Wu W, Li R, Li X, He J, Jiang S, Liu S, et al. Quercetin as an Antiviral Agent Inhibits Influenza A Virus (IAV) Entry. Viruses. 2015;**8**(1):6. https://www.ncbi.nlm.nih.gov/pmc/articles/PMC4728566/

[45] Jia S, Shen M, Zhang F, Xie J. Recent advances in *Momordica charantia*: Functional components and biological activities. International Journal of Molecular Sciences. 2017;**18**(12):2555

[46] Malainer C, Schachner D, Sangiovanni E, Atanasov AG, Schwaiger S, Stuppner H, et al. Eurycomalactone inhibits expression of endothelial adhesion molecules at a post-transcriptional level. Journal of Natural Products. 2017;**80**:3186–3193

[47] Yunos NM, Wahab HA, Al-Thiabat MG, Sallehudin NJ, Jauri MH. In vitro and In silico analysis of the anticancer effects of eurycomanone and eurycomalactone from *Eurycoma longifolia*. Plants. 2023;**12**(15):2827–7

[48] Zekri A, Ouassaf M, Khan SU, Rengasamy KRR, Alhatlani BY. Discovery of novel natural inhibitors of H5N1 neuraminidase using integrated molecular modeling and ADMET prediction. Bioengineering. 2025;**12**(6):622. https://www.mdpi.com/2306-5354/12/6/622

[49] McAuley JL, Gilbertson BP, Trifkovic S, Brown LE, McKimm-Breschkin JL. Influenza virus neuraminidase structure and functions. Frontiers in Microbiology. 2019;**10**(39). https://www.ncbi.nlm.nih.gov/pmc/articles/PMC6362415/

[50] Dong Y, Liao M, Meng X, Somero GN. Structural flexibility and protein adaptation to temperature: Molecular dynamics analysis of malate dehydrogenases of marine molluscs. Proceedings of the National Academy of Sciences. 2018;**115**(6):1274–1279

[51] Oyewusi HA, Huyop F, Wahab RA, Hamid A. In silico assessment of dehalogenase from bacillus thuringiensis H2 in relation to its salinity-stability and pollutants degradation. Journal of Biomolecular Structure and Dynamics. 2021;**40**(19):9332–9346

[52] Sanches BMA, Ferreira EI. Is prodrug design an approach to increase water solubility? International Journal of Pharmaceutics. 2019;**568**:118498. DOI: 10.1016/j.ijpharm.2019.118498

[53] Sorkun MC, Khetan A, Er S. AqSolDB, a curated reference set of aqueous solubility and 2D descriptors for a diverse set of compounds. Scientific Data. 2019;**6**(1):143

[54] Falcón-Cano G, Molina C, Cabrera-Pérez MÁ. Reliable prediction of caco-2 permeability by supervised recursive machine learning approaches. Pharmaceutics. 2022;**14**(10):1998

[55] Pyatigorskaya NV, Kravchenko AD. Caco-2 intestinal permeability study of

phenyltetrahydroquinolinedione derivative–TRPA1 antagonist. Drug Development and Registration. 2022;**11** (3):195–201

[56] Antonescu IE, Rasmussen KF, Neuhoff S, Fretté X, Karlgren M, Bergström CAS, et al. The permeation of Acamprosate is predominantly caused by paracellular diffusion across caco-2 cell monolayers: A paracellular modeling approach. Molecular Pharmaceutics. 2019;**16**:4636–4650

[57] Mohamed SS, Bensaber SM, Meiqal NH, Hermann A, Gbaj AM. Design and in-silico evaluation of pyridine-4-carbohydrazide derivatives for potential therapeutic applications. Journal of Surgical Case Reports and Images. 2025;**8**(3):235. DOI: 10.31579/2690-1897/235

[58] Olatunde A, Sulaiman U, Muhammad BB, Tijjani H, Muktar MA, Ibiyemi BF, et al. Deciphering the inhibitory activity of flavonoids against plasmodium falciparum proteases through molecular docking, drug-likeness and pharmacokinetic studies. Discover Chemistry. 2025;**2** (1):294. DOI: 10.1007/s44371-025-00339-0

[59] Ahmmed R, MdB H, Ajadee A, Mahmud S, MdA A, MdMH M, et al. Bioinformatics analysis to disclose shared molecular mechanisms between type-2 diabetes and clear-cell renal-cell carcinoma, and therapeutic indications. Scientific Reports. 2024;**14**(1):19133. DOI: 10.1038/s41598-024-69302-w

[60] Lombardo F, Bentzien J, Berellini G, Muegge I. In silico models of human PK parameters. prediction of volume of distribution using an extensive data set and a reduced number of parameters. Journal of Pharmaceutical Sciences. 2020;**110** (1):500–509. https://jpharmsci.org/article/S0022-3549(20)30493-7/fulltext

[61] Watanabe R, Esaki T, Kawashima H, Natsume-Kitatani Y, Nagao C, Ohashi R, et al. Predicting fraction unbound in human plasma from chemical structure: Improved accuracy in the low value ranges. Molecular Pharmaceutics. 2018;**15**:5302–5311

[62] Wanat K, Brzezińska E. Chromatographic data in statistical analysis of BBB permeability indices. Membranes. 2023;**13**(7):623–3. https://www.mdpi.com/2077-0375/13/7/623

[63] Ekowati J, Diyah NW, Nofianti KA, Hamid IS, Siswandono S. Molecular docking of ferulic acid derivatives on P2Y12 receptor and their ADMET prediction. Journal of Mathematical and Fundamental Sciences. 2018;**50**(2):203–219

[64] Stéen EJL, Vugts DJ, Windhorst AD. The application of in silico methods for prediction of blood-brain barrier permeability of small molecule PET tracers. Frontiers in Nuclear Medicine. 2022;**2**:853475. DOI: 10.3389/fnume.2022.853475

[65] Wright SH. Molecular and cellular physiology of organic cation transporter 2. American Journal of Physiology-Renal Physiology. 2019;**317** (6):F1669–79

[66] Noga M, Jurowski K. ADME of bromo-dragonfly as an Example of a New Psychoactive Substance (NPS) – application of in silico methods for prediction: Absorption, distribution, metabolism and excretion. Scientific Reports. 2025;**15**(1):22949. DOI: 10.1038/s41598-025-06453-4

[67] Sidhic J, Singh MT, Sarbadhikary P, Arunaksharan N, SC T, Krishnamurthy PT, et al. Phytochemical and Pharmacokinetic Evaluation of Humboldtia sanjappae: LC-MS/MS Profiling, ADMET Predictions, and in Vivo Toxicity Assessment. SSRN [Preprint]. 2025

[68] Su S, Sun J, Wang Y, Xu Y. Cardiac hERG K+ channel as safety and pharmacological target. Pharmacology of Potassium Channels. 2021;**267**: 139–166. DOI: 10.1007/164_2021_455

[69] Bakhdar F. The role of CYP 450 isozymes in drug-drug interaction. Journal of Umm Al-Qura University for Medical Sciences. 2020;**6**(1):36–40

[70] Ye N, Yang Z, Liu Y. Applications of Density Functional Theory in COVID-19 Drug Modeling. Drug Discovery Today. 2021;**27**(5):1411–1419. DOI: 10.1016/j.drudis.2021.12.017

[71] Zhang Y, Gao H, Liang W, Tang L, Yang Y, Wu X, et al. Efficacy of oseltamivir-peramivir combination therapy compared to oseltamivir monotherapy for Influenza A (H7N9) infection: A retrospective study. BMC Infectious Diseases. 2015;**16**(1):76. DOI: 10.1186/s12879-016-1383-8